

The Propeller and the Frog

Margaret Pan¹ and Eugene Chiang^{1,2}

mpan@astro.berkeley.edu

ABSTRACT

“Propellers” in planetary rings are disturbances in ring material excited by moonlets that open only partial gaps. We describe a new type of co-orbital resonance that can explain the observed non-Keplerian motions of propellers. The resonance is between the moonlet underlying the propeller, and co-orbiting ring particles downstream of the moonlet where the gap closes. The moonlet librates within the gap about an equilibrium point established by co-orbiting material and stabilized by the Coriolis force. In the limit of small libration amplitude, the libration period scales linearly with the gap azimuthal width and inversely as the square root of the co-orbital mass. The new resonance recalls but is distinct from conventional horseshoe and tadpole orbits; we call it the “frog” resonance, after the relevant term in equine hoof anatomy. For a ring surface density and gap geometry appropriate for the propeller Blériot in Saturn’s A ring, our theory predicts a libration period of ~ 4 years, similar to the ~ 3.7 year period over which Blériot’s orbital longitude is observed to vary. These librations should be subtracted from the longitude data before any inferences about moonlet migration are made.

Subject headings: planetary rings, planets and satellites

1. INTRODUCTION

Satellites embedded within planetary rings open gaps (Goldreich & Tremaine 1980). Ring particles passing by a satellite are gravitationally repelled so that the satellite is surrounded by an underdensity of ring material. In Saturn’s rings, satellites larger than a few km open gaps extending a full 2π radians in azimuth (e.g., Pan in the Encke gap;

¹Department of Astronomy, University of California, Berkeley, CA 94720

²Department of Earth and Planetary Science, University of California, Berkeley, CA 94720

Showalter et al. 1986). For smaller moonlets, physical collisions and gravitational interactions between ring particles diffuse particles back into the gap downstream of the moonlet. Thus partial gaps are produced whose azimuthal extents depend on ring viscosity and moonlet mass (Spahn & Sremčević 2000; Sremčević et al. 2002; Seiß et al. 2005; Lewis & Stewart 2009).

The *Cassini* spacecraft has imaged such partial gaps (Tiscareno et al. 2006; Sremčević et al. 2007; Tiscareno et al. 2008; Tiscareno et al. 2010, hereafter T10). Because of Keplerian shear, density perturbations excited at a moonlet’s position drift toward greater longitudes inside the moonlet’s orbit and toward lesser longitudes outside, forming a pair of features dubbed a “propeller” for its S-like shape. According to numerical simulations, a propeller’s radial width (the radial offset between the azimuthally extended propeller “blades”) is $\delta r \sim 4$ Hill radii of the moonlet (Seiß et al. 2005; Lewis & Stewart 2009). Combining this result with measurements of propellers’ radial widths from *Cassini* images, T10 infer moonlet radii of $\sim 0.1\text{--}1$ km.

The appearance of a given propeller varies significantly from image to image, depending on the illumination and viewing geometries, the 3D structure of the density perturbations, and the optical properties of ring particles. These effects have not yet been disentangled. Still, it seems clear that at least for some propellers, the gaps’ azimuthal (longitudinal) lengths are much larger than their radial widths. Panel (e) of Figure 1 of T10 shows an S-shaped bright lobe of radial width $\delta r \sim 5.5$ km and azimuthal length ~ 100 km—this is the propeller Blériot, the largest and most extensively imaged—embedded within a still longer dark gap whose azimuthal half-length (half the distance between gap ends) is $L_\phi \sim 500$ km ~ 300 Hill radii.

Intriguingly, Blériot displays non-Keplerian motion (T10). Over several years, Blériot’s orbital longitude deviated from a strictly Keplerian solution, showing residuals that varied nearly sinusoidally in time with a period of ~ 3.7 yr and an amplitude (half the distance from peak to trough) of ~ 0.1 deg or ~ 200 km, an amount less than but of order L_ϕ . Data for other propellers are much more limited than for Blériot but suggest similar behavior (T10).

The longitude variations imply semimajor axis variations of the underlying moonlet. Crida et al. (2010) and Rein & Papaloizou (2010) investigated semimajor axis variations due to stochastic torques exerted by self-gravitating wakes of ring particles (Salo 1995). Over timescales of years, stochastic torques might give rise to observable drifts in longitude, as shown in Figure 6 of Rein & Papaloizou (2010). But the observed 3.7-year period of the longitude variations does not arise naturally from stochastic torques, which are driven

by wakes that have lifetimes of order one orbit period $\simeq 14$ hours.¹ Alternatively, Blériot’s moonlet may librate within a resonance established by another larger moon (T10). However, no such resonant partner has been identified. Furthermore, many other propellers show longitude deviations of similar magnitude to Blériot’s, and invoking a separate partner moon for every propeller seems unnatural.

Here we propose that Blériot and propellers like it are indeed participating in resonances. But the resonances are with nearby ring material, not with other moons. Each propeller’s moonlet librates within the potential established by co-orbiting ring particles at the ends of the long gaps, at distances L_ϕ away. This new type of co-orbital resonance, reminiscent of that between the Saturnian satellites Janus and Epimetheus (Yoder et al. 1983), shares properties with both tadpole and horseshoe orbits in the restricted three-body problem (see, for example, Murray & Dermott 1999).

2. THE FROG RESONANCE

We begin with a toy model of the co-orbital material (Figure 1a): two identical point masses (“secondaries”) each of mass $\mu/2 \ll 1$ orbiting a central body (“primary”) of mass 1. The secondaries reside on circular, co-planar, Keplerian orbits of radius 1 and angular frequency 1. The azimuthal separation of the secondaries is $2\phi \ll 2\pi$. The secondaries are meant to represent ring material at the ends of the gap opened by a propeller-moonlet.

The secondaries establish an equilibrium point between them at azimuth $\theta = 0$ and radius $r \simeq 1$ (in cylindrical coordinates in the frame co-rotating with the secondaries). Just as for the triangular Lagrange points, this equilibrium point is dynamically stable because of the Coriolis force. And as with conventional tadpole and horseshoe orbits, test particle motions about our equilibrium point decompose into a fast epicycle of period 2π and a slow libration of the guiding center (semimajor axis). We propose that the slow libration is the non-Keplerian motion reported by T10.

We now derive the libration period and the shape of the guiding center orbit in the limit of small libration amplitude. In the frame rotating with angular frequency 1, the equations

¹Crida et al. (2010) and Rein & Papaloizou (2010) completed their studies before Figure 4 of T10 was made public.

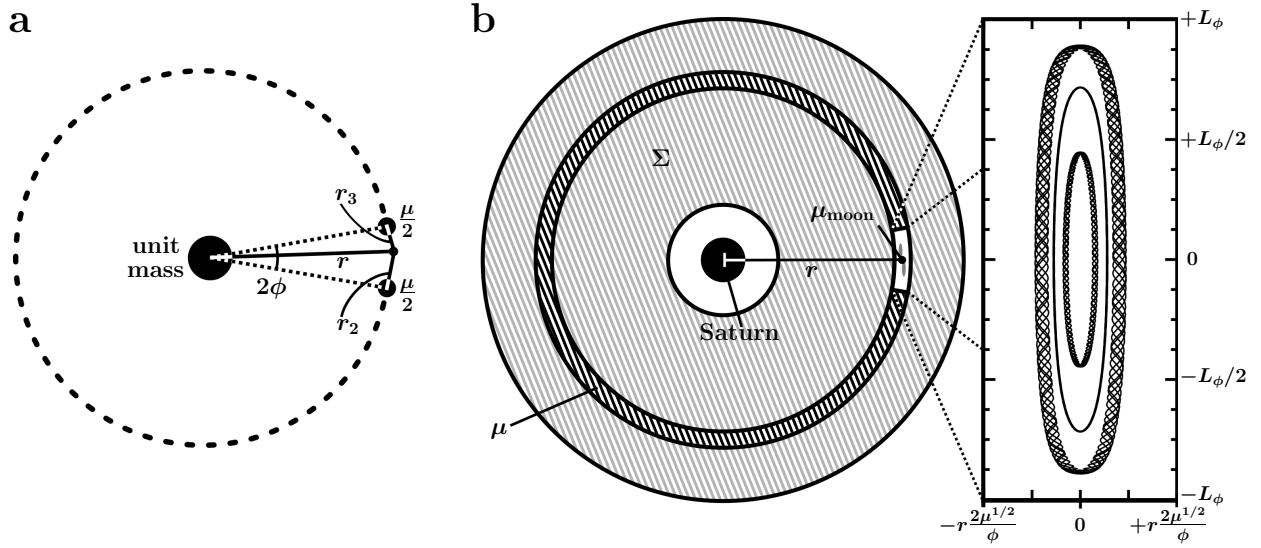


Fig. 1.— Schematic of our dynamical model for Saturnian propellers. Panel (a) depicts our toy model: a test-particle moonlet moving between two co-orbiting point-mass secondaries. All lengths and angles are evaluated in the frame co-rotating with the secondaries. Panel (b) illustrates how the propeller—the S-shaped figure centered on the moonlet—is embedded in a partial gap within Saturn’s rings. The point masses in panel (a) represent the ends of the heavily shaded, horseshoe-shaped, co-orbital ring in panel (b). The zoomed-in panel on the right shows sample trajectories of a test particle computed with the co-orbital mass distributed uniformly in azimuth outside the gap (see also Figure 2b) using $\mu = 10^{-4}$ and $L_\phi/r = 0.4$. Fast epicyclic motion of different amplitudes is visible on top of the azimuthally elongated “frog” orbit of the guiding center.

of motion for the (assumed massless) moonlet read

$$\ddot{r} - r\dot{\theta}^2 - 2r\dot{\theta} = \frac{\partial U}{\partial r} \quad (1)$$

$$r\ddot{\theta} + 2\dot{r}\dot{\theta} + 2\dot{r} = \frac{1}{r} \frac{\partial U}{\partial \theta} \quad (2)$$

where U is the celestial mechanician's potential,

$$U = \frac{1}{r} + \frac{\mu}{2r_2} + \frac{\mu}{2r_3} + \frac{1}{2}r^2, \quad (3)$$

and the distances between the moonlet and the secondaries are

$$r_2 = \sqrt{1 + r^2 - 2r \cos(\theta + \phi)}, \quad r_3 = \sqrt{1 + r^2 - 2r \cos(\theta - \phi)}. \quad (4)$$

Note that we are ignoring the displacement of the center-of-mass from the primary. As shown below, the associated indirect term of the potential, though crucial for the stability of conventional tadpoles, is not essential for our problem. Moreover, in the more realistic situation where the mass in the secondaries is spread smoothly over the co-orbital region—i.e., over nearly the full 2π rad in azimuth, excepting the gap of width 2ϕ —the barycentric displacement is much smaller than in the present two-point-mass problem. We will consider this more realistic case at the end of this section.

We expand U in the limit of small displacements from the equilibrium point, $\Delta \equiv r - 1 \ll 1$ and $\theta < \phi \ll \pi$:

$$U \approx \frac{3}{2} + \frac{3}{2}\Delta^2 + \frac{\mu}{\phi} \left(1 - \frac{\Delta}{2} - \frac{\Delta^2}{2\phi^2} + \frac{\theta^2}{\phi^2} \right). \quad (5)$$

We insert (5) into (1)–(2), taking $d/dt \ll 1$ and keeping only leading-order terms to filter out the fast epicyclic motion. We also assume that $\phi \gg \mu^{1/3}$, i.e., we assume that the gap length is much larger than the Hill sphere of the secondary (not to be confused with the Hill sphere of the moonlet). The fixed point is then

$$\Delta \simeq \frac{\mu}{6\phi}, \quad \theta = 0 \quad (6)$$

and the equations of motion about it are

$$\dot{\theta} = -3\Delta/2 \quad (7)$$

$$\ddot{\theta} + 2\dot{\Delta} = (2\mu/\phi^3)\theta. \quad (8)$$

Equation (7) states that the test particle moves according to the Kepler shear. Taking the time derivative of (7) and inserting the result into (8), we have

$$\ddot{\theta} = -(6\mu/\phi^3)\theta \quad (9)$$

which yields harmonic motion of period

$$P_{\text{lib}} = \frac{\pi\sqrt{2}}{\sqrt{3}} \frac{\phi^{3/2}}{\mu^{1/2}} \quad \text{for two point-mass secondaries} \quad (10)$$

in units where 2π is the local orbital period. Since Δ is largest when $\dot{\theta}$ is largest, the aspect ratio of the guiding center orbit is

$$\frac{\max \Delta}{\max \theta} = \frac{4}{\sqrt{6}} \frac{\mu^{1/2}}{\phi^{3/2}} \quad \text{for two point-mass secondaries.} \quad (11)$$

Numerical integrations of the two point-mass case agree well with equations (10) (Figure 2a) and (11) (data not shown).

A few comments:

1. As with conventional horseshoe orbits but not conventional tadpoles, stable librations here do not require the indirect potential.
2. As shown in Figure 2a, the libration period decreases with increasing libration amplitude; again, this behavior resembles that of horseshoes but not of tadpoles.
3. Without the Coriolis force term $2\dot{\Delta}$ in equation (8), stable librations would not occur. Thus the Coriolis force acts as a restoring force, just as it does for tadpoles.
4. Like the triangular Lagrange points, our fixed point corresponds to a local minimum of U and a local maximum of the physical potential $-U$. If the energy of a particle in resonance is dissipated slowly compared to the libration period, the libration amplitude should grow with time, just as for conventional tadpoles. Our numerical simulations confirm this.
5. Given $\phi \gg \mu^{1/3}$, the guiding center orbit is thinner in r than in θ . Conventional tadpole orbits are even thinner: $(\max \Delta / \max \theta)_{\text{tadpole}} = \sqrt{3\mu}$.

Given these commonalities with tadpoles and horseshoes, we refer to our guiding center orbits as “frog orbits.”²

We now address the more realistic situation where the secondary masses are spread uniformly in azimuth to fill the region $\theta = \phi$ to $\theta = 2\pi - \phi$ (passing through π). In this

²The rearward portion of a horse’s hoof—what would lie in the space between the ends of a horseshoe—is called a frog. See, e.g., <http://www.horsemanmagazine.com/wp-content/uploads/2008/09/horse-hoof-frog.jpg>.

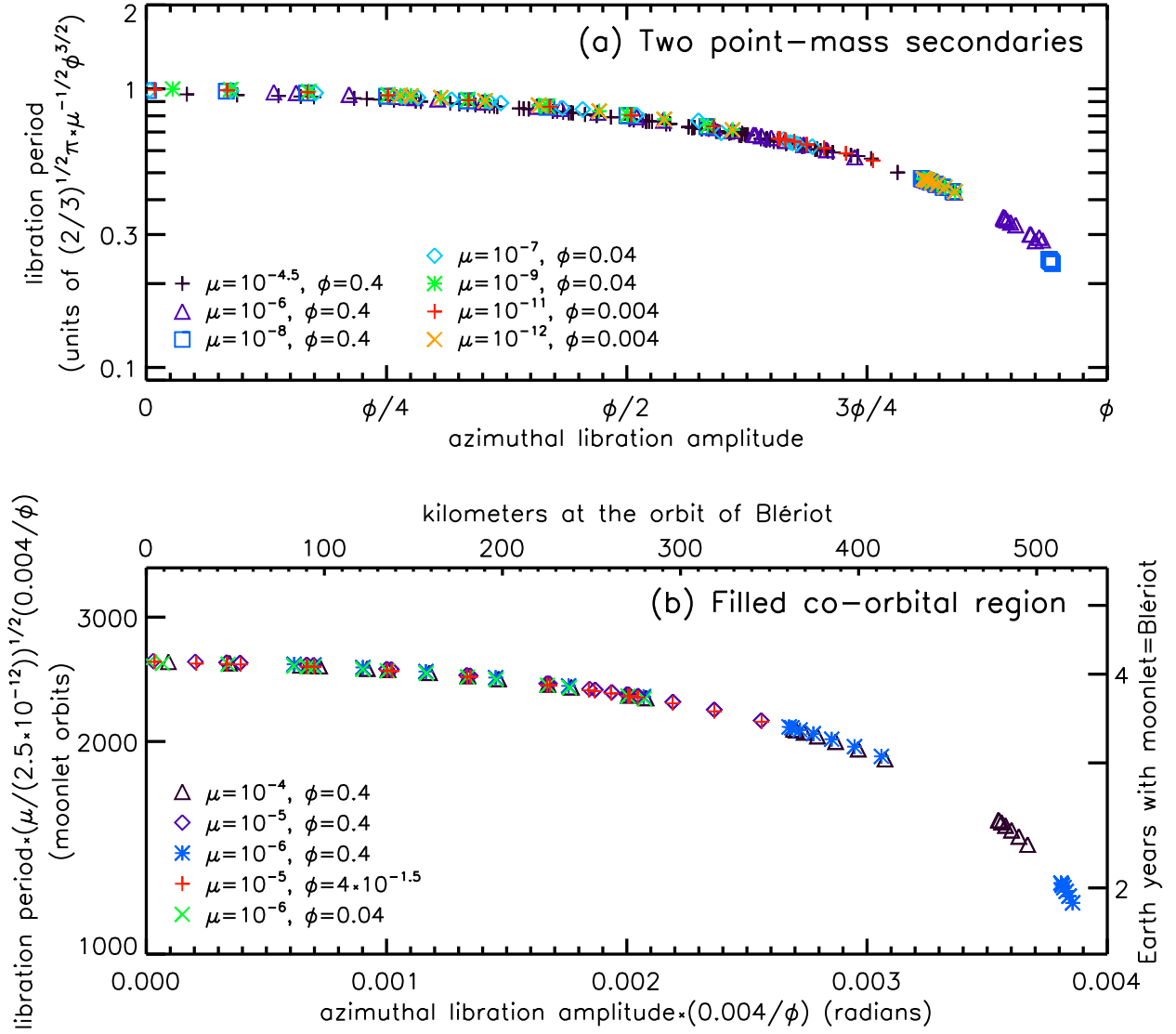


Fig. 2.— Libration period of a test particle as a function of azimuthal libration amplitude, computed from direct numerical integrations for a variety of co-orbital masses μ and gap azimuthal half-widths ϕ . (a) Results for the toy model with two point-mass secondaries. The y-axis is scaled to μ and ϕ according to equation (10), whose validity is confirmed by the data for small libration amplitude. (b) Results for the smoothed-out case where the co-orbital mass μ is modeled as a line source of uniform mass density extending in azimuth from ϕ to $2\pi - \phi$ (passing through π ; see Figure 1). The y-axis is scaled according to equation (12); that all data fall on the same curve confirms the scalings of this equation. Note that in both the two-point-mass and smoothed-out models, libration periods decrease as the libration amplitude increases. This behavior is similar to that of conventional horseshoe orbits.

case we might expect only the mass within an angle $\sim\phi$ of either end of the gap to influence the moonlet. In other words, the effective mass of the co-orbital region may be contained at azimuths $|\theta|$ between ϕ and $\sim 2\phi$. If so, then the scalings in equations (10) and (11) still apply with μ replaced by the effective mass $\sim(\phi/\pi)\cdot\mu$, where now μ is the mass of the entire ring co-orbiting with the moonlet. Our numerical simulations (Figures 1b, 2b) confirm the resulting scalings of period and aspect ratio with μ and ϕ and yield coefficients such that

$$P_{\text{lib}} \simeq 6.4 \frac{\phi}{\mu^{1/2}} \quad (12)$$

$$\frac{\max \Delta}{\max \theta} \simeq 0.7 \frac{\mu^{1/2}}{\phi} \quad \text{for } \mu \equiv \text{mass of entire co-orbital ring} \quad (13)$$

in the limit of small libration amplitude. For parameters inspired by Blériot and its environment—i.e., for $\phi = L_\phi/r \sim 500 \text{ km}/135000 \text{ km} \sim 0.004$ and $\mu \sim 2\pi\Sigma r \delta r/M_{\text{Saturn}} \sim 2.5 \times 10^{-12}$, where $\Sigma \sim 30 \text{ g cm}^{-2}$ is the disk surface density (Colwell et al. 2009) and $\delta r \sim 5.5 \text{ km}$ —our numerical integrations yield $P_{\text{lib}} \sim 4 \text{ yr}$. This is encouragingly close to the $\sim 3.7 \text{ yr}$ period measured by T10. Note that these parameters satisfy the assumptions $\mu \ll 1$, $\mu^{1/3} \ll \phi \ll 1$, and $\Delta < \delta r \ll 1$ that we made to derive equations (10)–(13). Also, assuming a moonlet density of $\sim 1 \text{ g/cc}$ and the median moonlet radius $\sim 0.75 \text{ km}$ inferred by T10, the moonlet-to-Saturn mass ratio μ_{moon} is $\sim 3 \times 10^{-15} \ll \mu$ as required by our assumption that the moonlet mass is negligible.

3. SUMMARY AND DISCUSSION

In this work we identified a new kind of orbital resonance between a moonlet embedded within an underdense gap of angular extent $\phi \ll \pi$ and disk material co-orbiting with the moonlet beyond the ends of the gap. We found formulae for the resonant libration period P_{lib} (equation 12) and the radial/azimuthal aspect ratio of the guiding center orbit (equation 13) in terms of ϕ and the co-orbital disk mass μ . These librations resemble standard tadpole orbits because $P_{\text{lib}} \propto 1/\mu^{1/2}$ and because the Coriolis force stabilizes the resonance. But whereas tadpoles also require the indirect potential for stability, the librations discussed here do not and are more like horseshoes in this respect. We propose that our new “frog resonance” explains the non-Keplerian motion seen for Saturnian propeller features such as Blériot. The observed timescale over which Blériot’s orbital longitude residuals vary ($\sim 3.7 \text{ yr}$) is well reproduced by our theory. Measurements of non-Keplerian motion and their interpretation as resonant frog librations thus offer new constraints on ring surface density (through μ) and gap geometry (through ϕ) independent of radiative transfer models of scattered light images.

Our simple resonance model does not include interactions with other satellites, nor does it account for disk torques responsible for Type I or Type II migration (for migration in the context of gas disks, see Ward 1997; analogous effects for particle disks like Saturn’s rings are discussed by, e.g., Crida et al. 2010). Since no propellers are seen at the locations of strong mean-motion resonances with the major Saturnian moons, and since Blériot at least has no obvious mean-motion resonant partner, we believe it reasonable to neglect such resonances. Secular interactions do not alter the semimajor axis of a propeller-moonlet; moreover, the eccentricities involved are too small for secular precession to be relevant.

Type I migration is driven by imbalanced Lindblad torques from the disks exterior and interior to the moonlet’s orbit. The torque from each side is dominated by material at the edge of the gap, located at a radial distance $\pm\delta r$ away from the moonlet. If we assume that the torque from the outer disk exceeds that from the inner disk by of order $\delta r/r$, where r is the moonlet’s orbital radius, then the Type I migration rate is given by

$$\dot{r}_{\text{Type I}} \sim -\mu_{\text{disk}} \cdot \mu_{\text{moon}} \cdot \left(\frac{r}{\delta r}\right)^2 \cdot v_{\text{Kepler}} \sim -1 \text{ cm/yr}, \quad (14)$$

where $\mu_{\text{disk}} = \Sigma r^2/M_{\text{Saturn}}$; Σ is the unperturbed local surface density; μ_{moon} is the mass ratio of the moonlet to Saturn; and v_{Kepler} is the Keplerian orbital velocity of the moonlet. Equation (14) follows from the standard impulse approximation (e.g., Dermott 1984). Because the gap radial width $\delta r \sim \mu_{\text{moon}}^{1/3} r$ for propellers, the scalings in equation (14) are equivalent to those of equation (39) of Crida et al. (2010): $\dot{r}_{\text{Type I}} \propto \mu_{\text{disk}} \mu_{\text{moon}}^{1/3} v_{\text{Kepler}}$. Our numerical estimate for $\dot{r}_{\text{Type I}}$ in equation (14) is made for parameters appropriate to Blériot and is much too small to contribute significantly to that propeller’s longitude residuals, as those residuals imply an rms radial speed of ~ 100 m/yr. Moreover the Type I drift is of one sign, whereas the radial drift of Blériot implied by the observations switches sign.

However, since $\delta r/r \sim 4 \times 10^{-5}$, the near cancellation of Lindblad torques assumed above is delicate and may be overwhelmed by radial surface density gradients. Any long-term trend in the longitude residuals, over and above the sinusoidal frog oscillations which we have analyzed, may therefore help constrain the radial density profile. For example, Figure 4a of Tiscareno et al. (2010) shows an apparent monotonic drift in Blériot’s longitude residuals of about $+0.05$ in 3.7 years. If this drift is real and if it grows quadratically with time—and these are highly uncertain prospects, as any characterization of a long-term trend depends on the method used to derive Blériot’s mean motion (M. Tiscareno, personal communication)—then such a drift would correspond to an inward migration speed of ~ 3 m/yr. The disk just outside Blériot’s orbit would have a greater surface density than that inside by of order 1 part in 100. Alternatively, a long-term nonlinear trend in the longitude could arise from the stochastic torques studied by Crida et al. (2010) and Rein & Papaloizou (2010).

We have interpreted the non-Keplerian motions of propeller-moonlets as backreactions of their perturbed disks on the moonlets. Our model, however, is not self-consistent because we have not considered how the motions of the moonlet feed back into shaping the gap. We have only computed the motion of a moonlet, idealized as a test particle, embedded in a gap whose structure is presumed stationary in the co-rotating frame. We do not have a theory that predicts the libration amplitude relative to the gap ends. Energy dissipation (for example, by interparticle collisions) tends to increase the libration amplitude, but we do not understand how the amplitude might be damped. Observationally, whether the gap itself shows non-Keplerian motion, or equivalently whether the moonlet moves relative to the gap ends, is difficult to determine (M. Tiscareno, personal communication). The appearance of a gap varies from image to image in ways not yet completely understood, and even measurements of basic quantities such as a gap’s angular size ϕ are complicated by azimuthal structure inside the gap (i.e., gap ends are not simple step functions). Improvements in radiative transfer modeling of images; more astrometric measurements of propellers and their relative positions inside their gaps; and a self-consistent theoretical treatment of how moonlets force disks and disks force moonlets may yield further insights.

We thank Matt Tiscareno for sharing his discovery in advance of publication that propellers exhibit non-Keplerian motion, and for subsequent discussions. MP appreciates the hospitality of the Canadian Institute for Theoretical Astrophysics, where part of the writing was done. We thank Glen Stewart for a helpful referee’s report, and Joe Burns for encouraging remarks. We thank Aurélien Crida, John Papaloizou, and Hanno Rein for feedback on our manuscript. This research was supported in part by the National Science Foundation and UC Berkeley’s Center for Integrative Planetary Science.

REFERENCES

- Colwell, J. E., Nicholson, P. D., Tiscareno, M. S., Murray, C. D., G., F. R., & Marouf, E. A. 2009, in *Saturn from Cassini-Huygens*, ed. M. Dougherty, L. Esposito, & T. Krimigis (Heidelberg: Springer), 375–412
- Crida, A., Papaloizou, J. C. B., Rein, H., Charnoz, S., & Salmon, J. 2010, *AJ*, 140, 944
- Dermott, S. F. 1984, in *IAU Colloq. 75: Planetary Rings*, ed. R. Greenberg & A. Brahic, 589–637
- Goldreich, P., & Tremaine, S. 1980, *ApJ*, 241, 425
- Lewis, M. C., & Stewart, G. R. 2009, *Icarus*, 199, 387

- Murray, C., & Dermott, S. 1999, *Solar System Dynamics* (Cambridge: Cambridge University Press)
- Rein, H., & Papaloizou, J. C. B. 2010, ArXiv e-prints
- Salo, H. 1995, *Icarus*, 117, 287
- Seiß, M., Spahn, F., Sremčević, M., & Salo, H. 2005, *Geophys. Res. Lett.*, 32, 11205
- Showalter, M. R., Cuzzi, J. N., Marouf, E. A., & Esposito, L. W. 1986, *Icarus*, 66, 297
- Spahn, F., & Sremčević, M. 2000, *A&A*, 358, 368
- Sremčević, M., Schmidt, J., Salo, H., Seiß, M., Spahn, F., & Albers, N. 2007, *Nature*, 449, 1019
- Sremčević, M., Spahn, F., & Duschl, W. J. 2002, *MNRAS*, 337, 1139
- Tiscareno, M. S., Burns, J. A., Hedman, M. M., & Porco, C. C. 2008, *AJ*, 135, 1083
- Tiscareno, M. S., Burns, J. A., Hedman, M. M., Porco, C. C., Weiss, J. W., Dones, L., Richardson, D. C., & Murray, C. D. 2006, *Nature*, 440, 648
- Tiscareno, M. S., Burns, J. A., Sremčević, M., Beurle, K., Hedman, M. M., Cooper, N. J., Milano, A. J., Evans, M. W., Porco, C. C., Spitale, J. N., & Weiss, J. W. 2010, *ApJ*, 718, L92
- Ward, W. R. 1997, *ApJ*, 482, L211+
- Yoder, C. F., Colombo, G., Synnott, S. P., & Yoder, K. A. 1983, *Icarus*, 53, 431